

Heating rate effects for the melting transition of Pt-Ag-Au nanoalloys

Hüseyin Yıldırım and Ali Kemal Garip

Citation: Chin. Phys. B, 2021, 30 (**10**): 108201. DOI: 10.1088/1674-1056/abee09
Journal homepage: http://cpb.iphy.ac.cn; http://iopscience.iop.org/cpb

What follows is a list of articles you may be interested in

Congruent melting of tungsten phosphide at 5 GPa and 3200℃ for growing its large single crystals

Xiao-Jun Xiang(向晓君), Guo-Zhu Song(宋国柱), Xue-Feng Zhou(周雪峰), Hao Liang(梁浩), Yue Xu(徐月), Shi-Jun Qin(覃湜俊), Jun-Pu Wang(王俊普), Fang Hong(洪芳), Jian-Hong Dai(戴建红), Bo-Wen Zhou(周博文), Wen-Jia Liang(梁文嘉), Yun-Yu Yin(殷云宇), Yu-Sheng Zhao(赵予生), Fang Peng(彭放), Xiao-Hui Yu(于晓辉), Shan-Min Wang(王善民)

Chin. Phys. B, 2020, 29 (**8**): 088202. DOI: 10.1088/1674-1056/ab928b

Performance optimization of self-powered visible photodetectors based on Cu_2O/electrolyte heterojunctions

Zhi-Ming Bai(白智明), Ying-Hua Zhang(张英华), Zhi-An Huang(黄志安), Yu-Kun Gao(高玉坤), and Jia Liu(刘佳)

Chin. Phys. B, 2020, 29 (**12**): 128202. DOI: 10.1088/1674-1056/abab7b

Design and management of lithium-ion batteries: A perspective from modeling, simulation, and optimization

Qian-Kun Wang(王乾坤), Jia-Ni Shen(沈佳妮), Yi-Jun He(贺益君), Zi-Feng Ma(马紫峰)

Chin. Phys. B, 2020, 29 (**6**): 068201. DOI: 10.1088/1674-1056/ab90f8

Angle-resolved x-ray photoelectron spectroscopy study of GeO_x growth by plasma post-oxidation

Zhiqian Zhao(赵治乾), Jing Zhang(张静), Xiaolei Wang(王晓磊), Shuhua Wei(魏淑华), Chao Zhao(赵超), Wenwu Wang(王文武)

Chin. Phys. B, 2017, 26 (**10**): 108201. DOI: 10.1088/1674-1056/26/10/108201

Densification and lithium ion conductivity of garnet-type $Li_{7-x}La_3Zr_{2-x}Ta_xO_{12}$ (x=0.25) solid electrolytes

Cao Yang, Li Yi-Qiu, Guo Xiang-Xin

Chin. Phys. B, 2013, 22 (**7**): 078201. DOI: 10.1088/1674-1056/22/7/078201

Heating rate effects for the melting transition of Pt–Ag–Au nanoalloys

Hüseyin Yıldırım[1,†] and Ali Kemal Garip[2]

[1] *Yenice Vocational School, Karabuk University, Karabuk, Turkey*
[2] *Department of Physics, Zonguldak Bulent Ecevit University, Zonguldak, Turkey*

(Received 25 January 2021; revised manuscript received 8 March 2021; accepted manuscript online 12 March 2021)

The classical molecular dynamics simulations in canonical NVT ensemble conditions are used to investigate the melting transition in different heating rates of Pt–Ag–Au ternary nanoalloys. In order to obtain the initial configurations used in the molecular dynamics simulations, optimizing the chemical ordering of $Pt_{13}Ag_nAu_{42-n}$ ($n = 0$–42) ternary nanoalloys was performed using the Basin–Hopping algorithm which would not allow changes in the icosahedron structure. The Gupta many-body potential was used to model interatomic interactions in both molecular dynamics simulations and optimization simulations. The melting transitions of selected Pt–Ag–Au nanoalloys were explored using caloric curves and Lindemann parameters. There have been two identified types of melting mechanisms, one includes sudden jump behavior in the caloric curve and the other is an isomerization while melting transition. The temperature range in which the isomerization takes place depends on the heating rate value.

Keywords: chemical ordering, melting, optimization, nanoalloys

PACS: 36.40.–c, 65.80.–g **DOI:** 10.1088/1674-1056/abee09

1. Introduction

Geometric shape, chemical ordering, size and composition dependent tunability of nanoalloys makes new nanoscale materials versatile and allows a fine tuning of specific properties such as optical, magnetic, and electronic properties.[1–3] In particular, chemical ordering of nanoalloys can help to design useful and inexpensive cost catalytic materials.[4] Therefore, high symmetry icosahedron nanoalloys organized in concentric core-shell structure are gaining increasing interest in catalysis applications due to the large surface-to-volume ratios that increase catalytic activity.[3,5,6] Also, it is important to know which atoms are located in the shell of a nanoalloy, because the surface strain between the core and shell atoms effects the catalytic activity.[4] In addition, if there is a core-shell nanoalloy in which shell atoms have the desired catalytic effects, it will be necessary to investigate the temperature range in which the nanoalloy remains thermally stable.[7] Some experimental studies in recent years show that Ag and Au surfaces change the catalytic activity. For example, Wang *et al.* reported that Ag surface segregation enhances the catalytic activity.[8] Li *et al.* obtained that more surface gold atoms have higher catalytic activity.[9] Christopher *et al.* studied the Ag (111) and (100) surfaces and found the higher selectivity of Ag (100) surface compared with Ag (111).[10] Zhu *et al.* examined the Ag (100), (110), (111) and (211) surfaces and found that the catalytic activity varied with the order of (110) > (100) > (111) > (211).[11] Woldu studied the Au (100), (110), and (111) surfaces and found that the (110) surface has the highest catalytic activity.[12] Mou *et al.* reported that the Au–Ag alloy catalyst has better catalytic activity than Au monometallic catalyst.[13,14] Zheng *et al.* found that the Au–Ag composition on the surface contributes more to the anaerobic benzyl alcohol dehydrogenation activity than the bulk.[15]

Direct methanol fuel cells (DMFC) and proton exchange membrane (PEM) fuel cells are promising technologies to reduce the dependence on fossil fuel energy due to its high energy conversion efficiency, clean energy and potential large-scale applications.[6,16–18] The performance of these fuel cells depends on low cost and the efficiency of the electrocatalysts which is the key component for the oxygen reduction reaction (ORR) and methanol oxidation reaction (MOR) in the PEM and DMFC fuel cells.[16,17,19,20] The most effective electrocatalysts for ORR and MOR are platinum (Pt) based nanoalloys due to their excellent reactivity and stability.[18–20] However, a few major drawbacks associated with Pt as a catalyst are expensive Pt reserves and limited availability.[21,22] Compared to pure and bimetallic Pt catalysts, Pt based ternary catalysts exhibit excellent catalytic activities in ORR and MOR and lower costs.[22,23] In this sense, to integrate Pt with other metals, Pt-based binary[24–27] and ternary[21,28–30] nanocatalysts have been extensively studied experimentally. Especially, crossover nanoalloys between the catalytically active group 10 (Ni, Pd, Pt) and the less active group 11 (Cu, Ag, Au) are important due to the fact that they can vary their surface structures and catalytic activity.[3,31] Moreover, adding Pt to Ag–Au binary nanoalloys dramatically increases the catalytic activity.[32] Some experimental results have shown that Pt–Ag–Au ternary

†Corresponding author. E-mail: huseyinyildirim@karabuk.edu.tr

© 2021 Chinese Physical Society and IOP Publishing Ltd

nanoalloys have improved catalytic activity.[21,33] Therefore, investigation of the structural and thermodynamic properties of Pt–Ag–Au ternary nanoalloys is important for future experimental studies in terms of their chemical and physical properties.

The reason for concentrating here on icosahedron structure is because the selected motif has highest symmetry of all discrete point groups and is only found in small clusters with a high surface to volume ratio.[34] Researchers chose 55-atom icosahedron as the model for the ternary nanoalloys due to the high symmetry and remarkable stabilization.[34,35] Furthermore, 55 is a geometric magic number for icosahedron structures that have quasi-spherical shape and close-packed surface, and exhibit significant structural and electronic stability.[3,5] Although structural and dynamic properties of pure, binary and ternary nanoalloys with Pt, Ag and Au with 55 atoms have been investigated in detail,[3–7,36–44] there is still lacking of studies of heating rate effects on melting process, and structural properties of Pt–Ag–Au ternary core-shell nanoalloys with 55 atoms.

Thus, in this study the structural properties and heating rate effect on the melting behaviors of 55-atom icosahedron $Pt_{13}Ag_nAu_{42-n}$ ($n = 0$–42) ternary nanoalloys are investigated systematically. The platinum atom number is fixed at 13 and the silver and gold atom numbers are varied for all other compositions. As a result of the structural optimization of 55-atom $Pt_{13}Ag_nAu_{42-n}$ ($n = 0$–42) ternary nanoalloys, the most stable composition is found. Then, in order to present the heating rate effect on the melting behaviors in detail, three different icosahedron compositions corresponding to $Pt_{13}Ag_{42}$, the most stable composition of $Pt_{13}Ag_nAu_{42-n}$ ($n = 0$–42) ternary nanoalloys and $Pt_{13}Au_{42}$ are selected. Thus, melting processes of Ag-rich, Au-rich and the most stable compositions are investigated.

2. Material and methods

The most stable chemical ordering of $Pt_{13}Ag_nAu_{42-n}$ ($n = 0$–42) ternary nanoalloys was obtained with the GMIN program[45] using the Basin–Hopping algorithm. The local relaxations for optimizing the chemical ordering were performed. The interatomic interactions were modeled by the Gupta potential[46,47] and Gupta parameters are given in Table 1.[48]

Table 1. The Gupta potential parameters for Pt–Ag–Au ternary nanoalloys.

	A (eV)	p	q	ξ (eV)	r_0 (Å)
Pt–Pt	0.2975	10.612	4.0040	2.6950	2.7747
Pt–Ag	0.1750	10.730	3.5900	1.7900	2.8330
Pt–Au	0.2500	10.420	4.0200	2.2000	2.8300
Ag–Ag	0.1031	10.850	3.1800	1.1895	2.8921
Ag–Au	0.1490	10.494	3.6070	1.4874	2.8864
Au–Au	0.2061	10.229	4.0360	1.7900	2.8840

The melting behaviors of nanoalloys were carried out by molecular dynamics (MD) simulations under canonical ensemble (NVT) conditions. All MD simulations have been carried out using the DL POLY 4 package.[49,50] The temperature was controlled by an Andersen thermostat with a relaxation time of 1.0 ps. Each nanoalloy was heated from 0 K to 1300 K with a temperature increment of 5 K. The best chemical ordering structures obtained as a result of the optimization of $Pt_{13}Ag_nAu_{42-n}$ ($n = 0$–42) ternary nanoalloys were taken as the initial configurations for MD simulations, and the melting temperatures of the nanoalloys were obtained to be dependent on the heating rate. Newton's equations of motion were integrated in 400000 steps using the velocity Verlet algorithm with 0.003 ps, 0.005 ps and 0.008 ps time steps. These simulation setups corresponds to a heating rate of 4.2 K/ns, 2.5 K/ns and 1.6 K/ns, respectively. To realize thermal equilibrium in MD, the total relaxation times for 1.6 K/ns, 2.5 K/ns and 4.2 K/ns heating rates are 3200 ps, 2000 ps and 1200 ps, respectively.

3. Results and discussion

In the current study, optimizing the chemical ordering was performed using the Basin–Hopping algorithm for 55-atom $Pt_{13}Ag_nAu_{42-n}$ ($n = 0$–42) ternary nanoalloys with an icosahedron structure. We mainly concentrate here on the $Pt_{13}Ag_nAu_{42-n}$ ($n = 0$–42) nanoalloys with fixed 13 Pt atoms where the fixed number 13 represents inner atoms of the 55-atom core-shell icosahedron structure.

Mixing energy (E_{mix}) analysis is a useful analysis method to the energetic stability among a family of nanoalloys with respect to composition. E_{mix} is defined as[5,51]

$$E_{\mathrm{mix}} = E\left(Pt_{13}Ag_nAu_{42-n}\right) - n\frac{E\left(Pt_{13}Ag_{42}\right)}{42} - (42-n)\frac{E\left(Pt_{13}Au_{42}\right)}{42}, \quad (1)$$

where $E\left(Pt_{13}Ag_nAu_{42-n}\right)$ represents the total energy of the ternary nanoalloy, $E\left(Pt_{13}Ag_{42}\right)$ and $E\left(Pt_{13}Au_{42}\right)$ represent the total energies of the bimetallic Pt–Ag and Pt–Au nanoalloys. Among all the compositions of nanoalloys, the structure in which the mixing energy takes the minimum value is more stable than the others. The mixing energies of $Pt_{13}Ag_nAu_{42-n}$ ($n = 0$–42) nanoalloys as a function of the number of Ag atoms (n) are shown in Fig. 1. From the mixing energy analysis, the lowest mixing energy value was obtained at the composition of $Pt_{13}Ag_{21}Au_{21}$ in $Pt_{13}Ag_nAu_{42-n}$ ($n = 0$–42) nanoalloys. In Fig. 1, blue, gray and yellow spheres represent platinum, silver and gold atoms, respectively.

Also, comparing the changing tendency of the number of Ag–Au bonds and the mixing energies as a function of Ag atoms in Fig. 1, we find that the two tendencies are adverse. In other words, the structures which contain more Ag–Au bonds

have lower mixing energies. This result indicates that composition with more Ag–Au bonds is more stable.

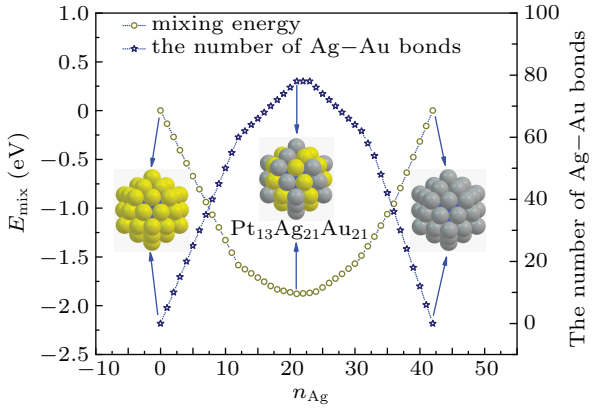


Fig. 1. Mixing energy variation and the number of Ag–Au bonds in $Pt_{13}Ag_nAu_{42-n}$ ($n = 0$–42) nanoalloys as a function of Ag atoms.

In order to better discuss the atomic mixing degree of different types of atoms in Pt–Ag–Au nanoalloys, the order parameter (R_A)[4] is adopted. R_A can be defined by the average distance of a type of atoms from the center of a cluster

$$R_A = \frac{1}{n_A}\sum_{i=1}^{n_A}\sqrt{x_i^2 + y_i^2 + z_i^2}, \tag{2}$$

where n_A is the number of atoms in each type in the ternary nanoalloys, and x_i, y_i and z_i show the positions of the atoms. Large R values indicate that the atoms are at the shell, while small R values indicate that the atoms are located in the core.

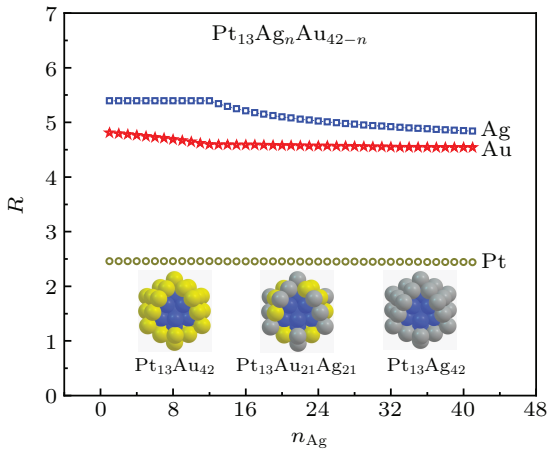


Fig. 2. The order parameter (R) variation of $Pt_{13}Ag_nAu_{42-n}$ ($n = 0$–42) nanoalloys.

From Fig. 3, it can be seen that R_{Ag} and R_{Au} are larger than R_{Pt} for all compositions, indicating that the locating tendencies of Ag and Au atoms to segregate to the shell and Pt atoms prefer to locate at core. For $n = 1$–12, R_{Ag} parameter keeps constant as 12 Ag atoms occupying the central sites of the shell. For $n = 13$–41, with the increase of Ag atoms, R_{Ag} decreases gradually and becomes closer to R_{Au} while R_{Au} almost remains constant. In addition, for $n = 1$–41, R_{Pt} almost remains constant. This means that the Pt atoms located at the core and Ag and Au atoms prefer to mix at the shell. Also, the segregation degrees of Pt, Ag and Au atoms in 55-atom Pt–Ag–Au ternary nanoalloys are mainly dependent on their surface energies, cohesive energies and atomic radii.

Table 2. Properties of Pt, Ag and Au.[31]

	Pt	Ag	Au
$r_{atomicradius}$ (Å)	1.385	1.445	1.44
$E_{cohesive}$ (eV)	5.84	2.95	3.81
$E_{surface}$ (meV·Å^{-2})	159	78	96.8

Owing to the large surface energy and cohesive energy, Pt atoms prefer to located in the core, while Ag and Au atoms prefer to locate on the shell as they have smaller surface energy and cohesive energy, in $Pt_{13}Ag_{42}$ and $Pt_{13}Au_{42}$ nanoalloys, respectively. Similarly, the core segregation of Pt is also associated with the lower atomic radius of Pt compared with Ag and Au. As a result, the Ag and Au atoms on the shell and the segregation of Pt atoms at the core enable minimization of the nanoalloy surface energy. The optimization results in general support the $Pt_{core}(AgAu)_{shell}$ that is proposed in this study. Also, Pacheco-Contreras *et al.* found the similar results for 13- and 19-atom icosahedron ternary Ag–Au–Pt nanoalloys.[48]

The melting temperature of a nanoalloy can be estimated by MD simulations. Also, the heating rate in MD simulations effects the melting transition of nanoalloys.[52] In this study, MD simulations were performed at three different heating rates for 55 atom $Pt_{13}Ag_{42}$, $Pt_{13}Ag_{21}Au_{21}$ and $Pt_{13}Au_{42}$ nanoalloys to investigate the effect of heating rate on the melting transition. The literature values of heating rate vary between 0.8 and 100 K/ns.[53–57] In the literature, the melting dynamics of the nanoalloy consisting of gold and silver atoms have studied with a heating rate of 10 K/ns.[54] In the present study, the heating rates were used as 1.6 K/ns, 2.5 K/ns and 4.2 K/ns. The caloric curve and the Lindemann index were used to clarify the melting transition.

The caloric curve and Lindemann index are commonly used in MD simulations to investigate melting behavior of nanoalloys. The caloric curve represents the total energy as a function of temperature and, melting temperature of the nanoalloy corresponds to distinguishable increase in total energy.[7] The melting temperatures of nanoalloys obtained from the caloric curve were also supported with the Lindemann index criteria. When the index is in the range of about 0.1–0.15, the melting occurs in nanoalloys, whereas the critical value can vary between 0.05–0.20 due to, e.g., the nature of interactions between atoms, the magnitude of quantum effects and the crystal structure.[5] For each layer, the Lindemann index is expressed as follows:[58,59]

$$\delta_{L(i)} = \frac{2}{N_{L(i)}(N_{L(i)}-1)}\sum_{j<k}\frac{\sqrt{\langle r_{jk}^2\rangle - \langle r_{jk}\rangle^2}}{r_{jk}}, \tag{3}$$

where $N_{L(i)}$ is the atom numbers in the i-th layer. r_{jk} is the distance between the j-th and k-th atoms. The 55-atom icosahedron nanoalloy consists of three layers starting from its center of mass. The 55-atom icosahedron nanoalloys have a single atom in the first layer, 12 atoms in the following second layer, and 42 atoms in the third layer.[7,44] The caloric curve and Lindemann index vary as a function of temperature during the heating processes for $Pt_{13}Au_{42}$, $Pt_{13}Ag_{21}Au_{21}$, $Pt_{13}Ag_{42}$ nanoalloys with different heating rates, as shown in Figs. 3, 5 and 6, respectively.

The caloric curve and Lindemann index of $Pt_{13}Au_{42}$ nanoalloys at heating rates of 1.6 K/ns, 2.5 K/ns vs. 4.2 K/ns, respectively, are shown in Fig. 3. In Fig. 3(a), the melting temperature of $Pt_{13}Au_{42}$ nanoalloy is 703 K due to the sudden jump in total energy. $Pt_{13}Au_{42}$ nanoalloy in Fig. 3(a) has dangling surface Au atoms at some temperatures according to Fig. 4(a). The dangling of these atoms effects the Lindemann index. The behaviors of the Lindemann index of each layer for $Pt_{13}Au_{42}$ and $Pt_{13}Ag_{21}Au_{21}$ are given in Fig. 4 to understand the melting mechanism with respect to layers. As shown in Fig. 4(a), the Lindemann index of the atoms on the shell of the nanalloy is greater than atoms in the core of the nanoalloy, which indicates that the shell atoms have large amplitude from their original lattice positions while the core atoms of nanoalloys remain their original lattice positions. It is also evident that an increase in temperature (595 K and 640 K) leads to a dangling in shell atoms. For $Pt_{13}Au_{42}$ nanoalloys in 2.5 K/ns and 4.2 K/ns heating rates, variations of the caloric curve and Lindemann index occur within a temperature range. Figures 3(b) and 3(c) show that this temperature range is small (60 K) for the heating rate of 4.2 K/ns and large (75 K) for the heating rate of 2.5 K/ns. Also, caloric curves and Lindemann indexes have abrupt changes in melting transition for the heating rates of 2.5 K/ns and 4.2 K/ns. This situation indicates that there is an isomerization caused by solid-liquid and liquid-solid transitions during the melting transition.

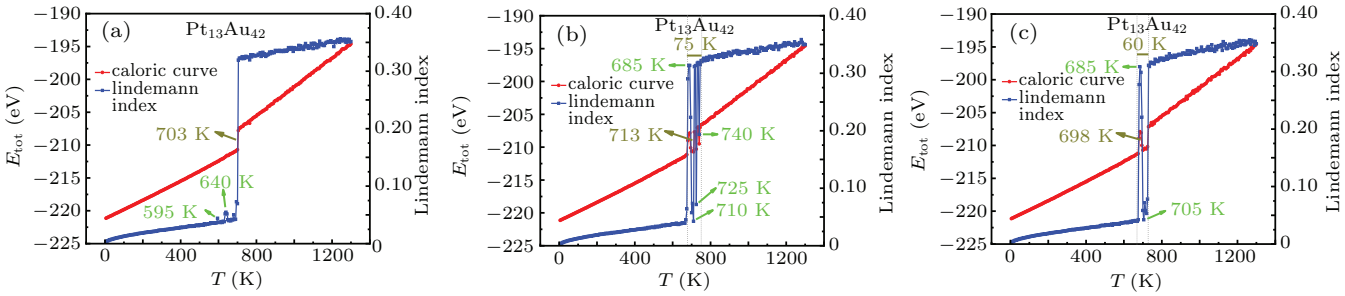


Fig. 3. The caloric curve and Lindemann index variation for $Pt_{13}Au_{42}$ nanoalloys at (a) 1.6 K/ns, (b) 2.5 K/ns and (c) 4.2 K/ns heating rates.

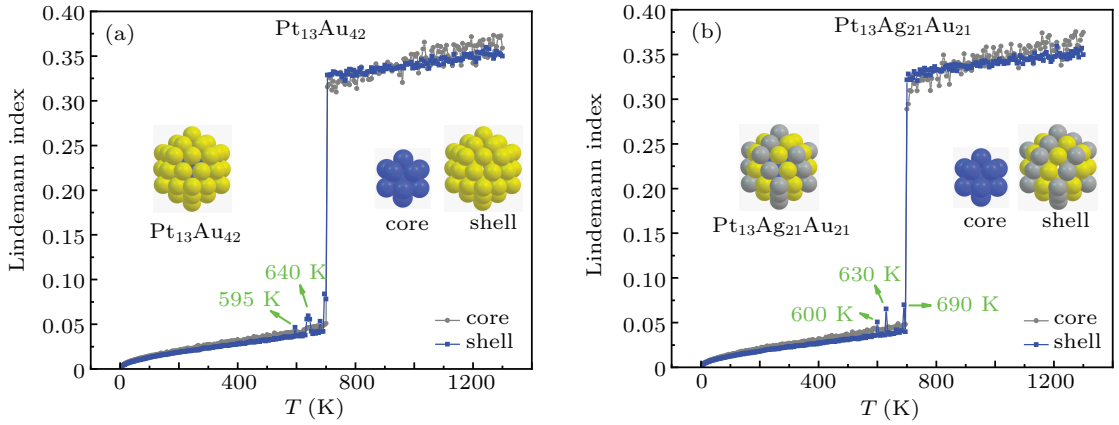


Fig. 4. Behavior of the layered Lindemann index for (a) $Pt_{13}Au_{42}$ and (b) $Pt_{13}Ag_{21}Au_{21}$ nanoalloys at 1.6 K/ns heating rate with respect to temperature.

Figure 5 shows the caloric curve and Lindemann index of $Pt_{13}Ag_{21}Au_{21}$ nanoalloys at heating rates of 1.6 K/ns, 2.5 K/ns and 4.2 K/ns, respectively. According to Figs. 5(a)–5(c), the melting temperature of the $Pt_{13}Ag_{21}Au_{21}$ nanoalloys is 698 K, 678 K, and 709 K due to the sudden jump in the Lindemann index and caloric curves. As shown in Fig. 5, melting temperature of $Pt_{13}Ag_{21}Au_{21}$ is lowest (678 K) in heating rate 2.5 K/ns. Also, there is no isomerization in Figs. 5(a)–5(c). The common characteristic of $Pt_{13}Ag_{21}Au_{21}$ nanoalloys with different heating rates is that they have dangling surface atoms before reaching the melting temperature. As shown in Fig. 4(b), it is observed that there are small movements in the Lindemann index and caloric curve because the melting sign of $Pt_{13}Ag_{21}Au_{21}$ nanoalloy starts from the surface.

The caloric curve and Lindemann index of $Pt_{13}Ag_{42}$ nanoalloys at heating rates of 1.6 K/ns, 2.5 K/ns and 4.2 K/ns, respectively, are shown in Fig. 6. The common characteristic of $Pt_{13}Ag_{42}$ nanoalloys with different heating rates is that

melting takes place within a temperature range. According to the Lindemann index in Fig. 6(a), the melting of $Pt_{13}Ag_{42}$ nanoalloy occurs between 668 K and 750 K, and there is an on-going isomerization in a range of 82 K. This is the smallest isomerization range for 55-atom $Pt_{13}Ag_{42}$ nanoalloys. As shown in Fig. 6(b), when the heating rate is 2.5 K/ns, the isomerization range is 168 K. There is a solid–liquid transition between 632 K and 800 K. In this temperature range of 168 K, the nanoalloy passed into the liquid phase and then turned into the solid phase again. This is the largest isomerization range for 55-atom $Pt_{13}Ag_{42}$ nanoalloys. In addition, when the heating rate is 4.2 K/ns, the isomerization range is 146 K. There is a solid-liquid transition between 708 K and 854 K. As a result, the temperature range where melting occurs are varies at different heating rate for $Pt_{13}Ag_{42}$ nanoalloys.

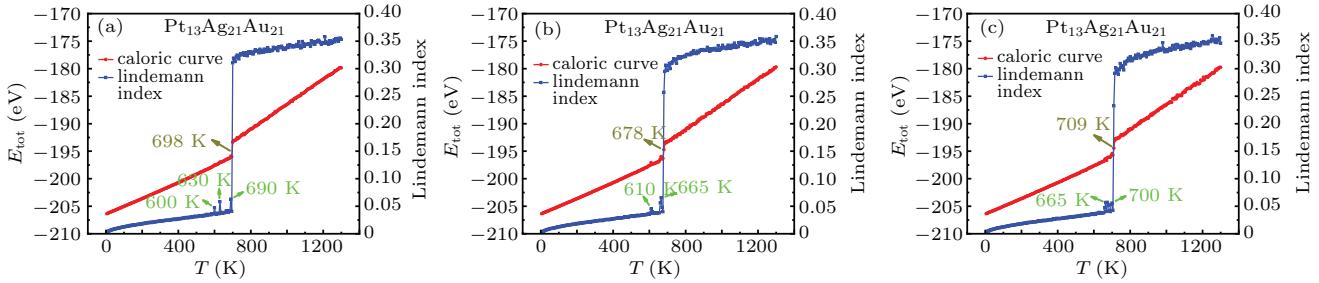


Fig. 5. The caloric curve and Lindemann index variation for $Pt_{13}Ag_{21}Au_{21}$ nanoalloys at (a) 1.6 K/ns, (b) 2.5 K/ns and (c) 4.2 K/ns heating rates.

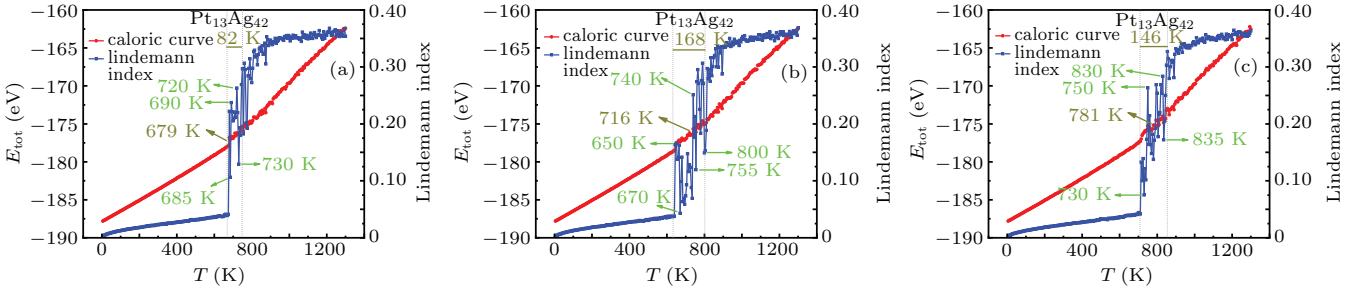


Fig. 6. The caloric curve and Lindemann index variation for $Pt_{13}Ag_{42}$ nanoalloys at (a) 1.6 K/ns, (b) 2.5 K/ns and (c) 4.2 K/ns heating rates.

In order to investigate the size effect, we selected some compositions for 147 and 309 atom clusters. The melting transitions have been examined by the caloric curves and Lindemann index variations for 400000 MD steps. The results are shown in Figs. 7 and 8. The outstanding behavior is the sudden jump behavior for selected Pt–Au and Pt–Ag–Au nanoalloys with 55, 147 and 309 atoms. There are other melting mechanisms which do not include sudden jump behavior, and a few examples are given in Figs. 3(b), 3(c), 6(a), 6(b), and 6(c). In addition, the melting temperatures of the 147 and 309 atoms were found to be relatively higher for the examined compositions as seen from Figs. 7 and 8.

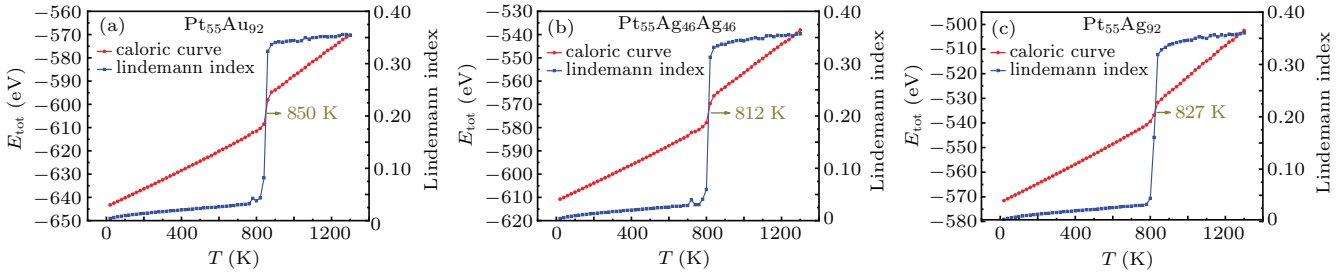


Fig. 7. The caloric curve and Lindemann index variation for nanoalloys of (a) $Pt_{55}Au_{92}$, (b) $Pt_{55}Ag_{46}Au_{46}$, and (c) $Pt_{55}Ag_{92}$.

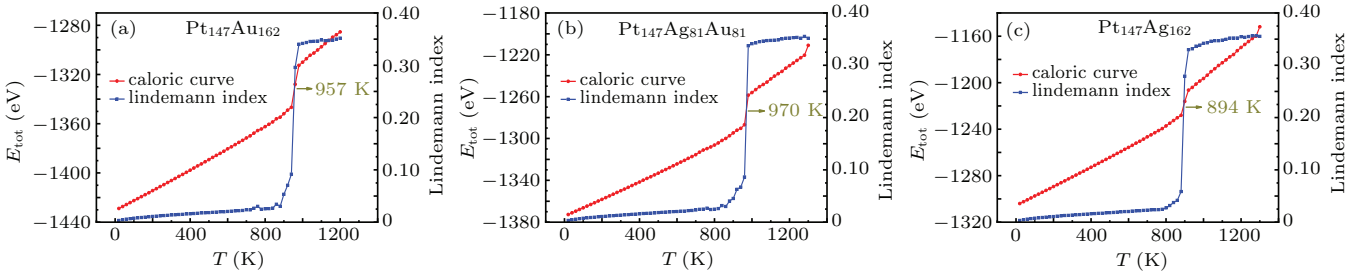


Fig. 8. The caloric curve and Lindemann index variation for nanoalloys of (a) $Pt_{147}Au_{162}$, (b) $Pt_{147}Ag_{81}Au_{81}$, and (c) $Pt_{147}Ag_{162}$.

The composition effect on the melting temperatures has been examined for 55-atom Pt–Ag–Au nanoalloys. The results are given in Fig. 9. It is found that the melting temperatures fluctuate between 653 K and 721 K depending on the composition. In this fluctuation, the highest and lowest melting temperatures belong to $Pt_{13}Ag_7Au_{35}$ and $Pt_{13}Ag_8Au_{34}$ compositions, respectively. In addition, two different melting mechanisms have been observed in binary nanoalloys as in ternary nanoalloys.

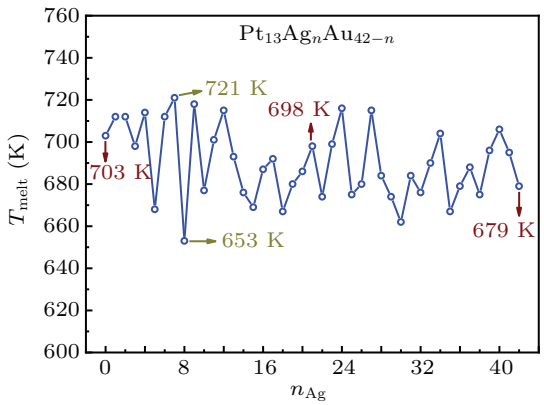


Fig. 9. The caloric curve and Lindemann index variation for $Pt_{13}Ag_nAu_{42-n}$ nanoalloys.

We used the Ackland–Jones analysis to see the structural changes (isomerization) during melting transitions of $Pt_{13}Au_{42}$ and $Pt_{13}Ag_{42}$ nanoalloys. The Ackland–Jones analysis is a tool to distinguish ICO, BCC, HCP, and FCC coordination structures based on analysis of the distribution of angles formed by the pairs of neighbors of a central atom.[60–62] In this method, at beginning, inner shell atoms of nanoalloy are described as HCP coordinated and all surface atoms are described as disordered.

We chose the configurations with isomerization which characterizes the structural evolution. The Ackland–Jones analysis of the configurations which are corresponding to $Pt_{13}Au_{42}$ and $Pt_{13}Ag_{42}$ compositions is presented in Tables 3 and 4, respectively. When we analyze the tables with the melting transition, the number of HCP coordinated atoms decreases and the number of disordered atoms increases. While this change in HCP coordinated atoms is slower in $Pt_{13}Au_{42}$ nanoalloys, it is abruptly decreased in $Pt_{13}Ag_{42}$ nanoalloys. Transitions from HCP coordinated atoms to BCC and FCC coordinated atoms correspond to isomerization at temperatures determined with the Lindemann criterion where the melting transition occurs. During the melting transition, the number of HCP coordinated atoms decreases and the number of BCC coordinated atoms changes. We also see that the number of FCC coordinated atoms varies slightly. This clearly shows that some of the HCP coordinated atoms change their local structure to BCC and FCC coordinations, as we do not see any important change in disordered atoms. In general, disordered atoms also dominate after the melting transitions.

Table 3. Structural evolution through the Lindemann index of $Pt_{13}Au_{42}$ nanoalloy in different heating rates.

	T (K)	FCC	HCP	BCC	ICO	Disordered
Heating rate 1.6 K/ns	0	0	12	0	1	42
	500	0	12	0	1	42
	700	0	11	0	1	43
	705	0	9	1	1	44
	710	1	4	4	1	45
	1000	1	3	2	3	46
	1300	0	2	5	0	48
Heating rate 2.5 K/ns	0	0	12	0	1	42
	500	0	12	0	1	42
	685	1	6	2	3	43
	710	1	10	1	1	42
	720	0	4	4	2	45
	725	0	11	0	1	43
	740	0	2	7	3	43
	1000	0	3	3	0	49
	1300	2	1	0	0	52
Heating rate 4.2 K/ns	0	0	12	0	1	42
	500	0	12	0	1	42
	685	1	7	3	1	43
	705	0	12	0	1	42
	730	0	4	4	2	45
	1000	2	5	1	0	47
	1300	0	4	0	0	51

Table 4. Structural evolution through the Lindemann index of $Pt_{13}Ag_{42}$ nanoalloy in different heating rates.

	T (K)	FCC	HCP	BCC	ICO	Disordered
Heating rate 1.6 K/ns	0	0	12	0	1	42
	500	0	12	0	1	42
	685	0	0	5	9	41
	690	1	0	1	12	41
	720	0	0	2	10	43
	730	1	4	2	9	39
	1000	1	2	2	4	46
	1300	0	3	1	0	51
Heating rate 2.5 K/ns	0	0	12	0	1	42
	500	0	12	0	1	42
	650	0	0	2	12	41
	670	0	1	2	10	42
	740	3	0	3	6	43
	755	0	1	3	7	44
	800	1	3	2	7	42
	1000	1	1	4	4	45
	1300	0	1	3	0	51
Heating rate 4.2 K/ns	0	0	12	0	1	42
	500	0	11	0	1	43
	730	0	2	1	11	41
	750	0	4	5	5	41
	785	3	1	2	3	46
	830	0	0	3	9	43
	835	2	1	2	7	43
	1000	0	0	2	9	44
	1300	0	2	2	0	51

4. Conclusions

In summary, we have performed a theoretical study of different compositions of icosahedral Pt–Ag–Au ternary nanoal-

loys using many-body Gupta potential. Using the chemical ordering optimization results of $Pt_{13}Ag_nAu_{42-n}$ (n = 0–42) nanoalloys, we have performed bond number and mixing energy analysis. The results show that the most stable composition is $Pt_{13}Ag_{21}Au_{21}$, which has the lowest mixing energy with highest number of Ag–Au bonds. Also, order parameter analysis indicates that Ag and Au atoms generally segregate at the shell and Pt atoms locate at the core of the nanoalloys, which is further explained by the atomic radius, surface energy and cohesive energy of bulk values of those elements. The chemical ordering optimization results in general support the $Pt_{core}(AgAu)_{shell}$, which is proposed in this study. MD simulations are used to investigate the heating rate effect on the melting transition of $Pt_{13}Au_{42}$, $Pt_{13}Ag_{21}Au_{21}$ and $Pt_{13}Ag_{42}$ ternary nanoalloys under NVT conditions. Also, in order to investigate the size effect, MD simulations of selected some compositions for 147 and 309 atom clusters have been performed. The melting transitions of selected Pt–Ag–Au nanoalloys are explored using caloric curves and Lindemann parameters. There have been two identified types of melting mechanisms, one includes sudden jump behavior in the caloric curve and the other includes some isomerisation through melting transition. A detailed investigation for melting transitions for the first type shows that just before transition temperature the surface atoms begin to dangle before core atoms. The temperature range in which the isomerization takes place depends on the heating rate value. Also, the melting temperatures of the 147 and 309 atoms are found to be relatively higher than 55 atoms for the examined compositions. In addition, the simulation results show that the melting temperatures of $Pt_{13}Ag_nAu_{42-n}$ (n = 0–42) nanoalloys fluctuate, depending on the composition. These results are of great importance for multifunctional properties of Pt–Ag–Au ternary nanoalloys.

Acknowledgement

DL_POLY_4 is a molecular dynamics simulation package written by I. T. Todorov and W. Smith, and has been obtained from STFC's Daresbury Laboratory via the website http://www.ccp5.ac.uk/DL_POLY.

References

[1] Cezar H M, Rondina G G and Da Silva J L F 2019 *J. Chem. Phys.* **151** 204301
[2] Taran S, Garip A K and Arslan H 2020 *Chin. Phys. B* **29** 077801
[3] Taran S 2020 *Sakarya University Journal of Science* **24** 501
[4] Taran S, Garip A K and Arslan H 2020 *J. Cluster Sci.* **32** 199
[5] Yildirim H and Arslan H 2020 *Int. J. Mod. Phys. C* **31** 2050078
[6] Taran S 2019 *Comput. Theor. Chem.* **1166** 112576
[7] Garip A K 2018 *Int. J. Mod. Phys. C* **29** 1850084
[8] Wang L C, Zhong Y, Jin H, Widmann D, Weissmüller J and Behm R J 2013 *Beilstein J. Nanotechnol.* **4** 111
[9] Li S, Chen H, Liu X, Liu H, Ma J and Zhu Y 2020 *Chem. Sci.* **11** 8000
[10] Christopher P and Linic S 2008 *J. Am. Chem. Soc.* **130** 11264
[11] Zhu L, Zhang W, Zhu J and Cheng D 2017 *App. Catal. A: General* **538** 27
[12] Woldu A R 2020 *Nanoscale* **12** 8626
[13] Liu J H, Wang A, Chi Y S, Lin H P and Mou C Y 2005 *J. Phys. Chem. B* **109** 40
[14] Liu X, Li Y, Lee J W, Hong C Y, Mou C Y and Jang B W L 2012 *Appl. Catal. A: General* **439–440** 8
[15] Zheng J, Qu J, Lin H, Zhang Q, Yuan X, Yang Y and Yuan Y 2016 *ACS Catal.* **6** 6662
[16] Xia Z, Li C M and Dai L 2019 *Matter* **1** 1445
[17] Noh S H, Han B and Ohsaka T 2015 *Nano Res.* **8** 3394
[18] Zhang H, Wang H, Cao J and Ni Y 2017 *J. Alloys Compd.* **698** 654
[19] Lan J, Li C, Liu T and Yuan Q 2019 *J. Saudi Chem. Soc.* **23** 43
[20] Wang X, Zhang L, Gong H, Zhu Y, Zhao H and Fu Y 2016 *Electrochim. Acta* **212** 277
[21] Thongthaia K, Pakawanitb P, Chenlekb N, Kimc J, Anantad S and Srisombat L 2017 *Nanotechnology* **28** 375602
[22] Tao J, Ji Q, Shao G, Li Z, Liu T and Wen Y 2017 *J. Alloys Compd.* **716** 240
[23] Fan T, Liu T, Zheng J, Shao G and Wen Y 2015 *J. Mater. Sci.* **50** 3308
[24] Cuevas-Muñiz F M, Gurrola M P, Tellez-Vazquez O, Esparza R, Guerra-Balcazar M, Arriaga L G and Ledesma-Garcia J 2015 *Int. J. Hydrogen Energy* **40** 17284
[25] Deng L, Hu W, Deng H and Xiao S 2010 *J. Phys. Chem. C* **114** 11026
[26] Kristian N and Wang X 2008 *Electrochem. Commun.* **10** 12
[27] Oliveira R C P, Sevim M, Sljukic B, Sequira C A C, Metin Ö and Santos D M F 2020 *Catal. Today* **357** 291
[28] Kang J, Chen T, Zhang D and Guo L 2016 *Nano Energy* **23** 145
[29] Wang M, He Y, Li R, Ma Z, Zhang Z and Wang X 2015 *Electrochim. Acta* **178** 259
[30] Fu G, Xia B, Ma R, Chen Y, Tang Y and Lee J 2015 *Nano Energy* **12** 824
[31] Ferrando R, Jellinek J and Johnston R L 2008 *Chem. Rev.* **108** 845
[32] Toshima N and Zhang H 2012 *Macromol. Symp.* **317** 149
[33] Zhang H, Okumura M and Toshima N 2011 *J. Phys. Chem. C* **115** 14883
[34] Ferrando R 2016 *Structure and Properties of Nanoalloys* in *Frontiers of Nanoscience* (Amsterdam: Elsevier) Vol. 10
[35] Echt O, Sattler K and Recknagel E 1981 *Phys. Rev. Lett.* **47** 1121
[36] Wu X and Sun Y 2017 *J. Nanopart. Res.* **19** 201
[37] Michaelian K, Rendon N and Garzon I L 1999 *Phys. Rev. B* **60** 2000
[38] Lambie S G, Weal G R, Blackmore C E, Palmer R E and Garden A L 2019 *Nanoscale Adv.* **1** 2416
[39] Wu X, Cai W and Shao X 2009 *J. Comput. Chem.* **30** 1992
[40] Chen F, Curley B C, Rossi G and Johnston R L 2007 *J. Phys. Chem. C* **111** 9157
[41] Arianfar F, Rostamian R and Behnejad H 2017 *Phys. Chem. Res.* **5** 359
[42] Piotrowski M J, Piquini P and Da Silva J L F 2012 *J. Phys. Chem. C* **116** 18432
[43] Zhao Z, Li M, Cheng D and Zhu J 2014 *Chem. Phys.* **441** 152
[44] Garip A K 2019 *Mol. Simul.* **45** 1004
[45] Wales D J and Doye J P K 1997 *J. Phys. Chem. A* **101** 5111
[46] Cleri F and Rosato V 1993 *Phys. Rev. B* **48** 22
[47] Gupta R P 1981 *Phys. Rev. B* **23** 6265
[48] Pacheco-Contreras R, Juárez-Sánchez J O, Dessens-Félix M, Aguilera-Granja F, Fortunelli A and Posada-Amarillas A 2018 *Comput. Mater. Sci.* **141** 30
[49] Bush I J, Todorov I T and Smith W 2006 *Comput. Phys. Commun.* **175** 323
[50] Todorov I T, Smith W, Trachenko K and Dove M T 2006 *J. Mater. Chem.* **16** 1911
[51] Datta S 2019 *AIP Adv.* **9** 115316
[52] Garip A K 2020 *Düzce Üniversitesi Bilim ve Teknoloji Dergisi* **8** 1732
[53] Arslan H, Garip A K and Taran S 2019 *J. Nanopart. Res.* **21** 130
[54] Gould A L, Logsdail A J and Catlow C R A 2015 *J. Phys. Chem. C* **119** 23685
[55] Chen F and Johnston R L 2008 *Appl. Phys. Lett.* **92** 023112
[56] Kuntová Z, Rossi G and Ferrando R 2008 *Phys. Rev. B* **77** 205431
[57] Mottet C, Goniakowski J, Baletto F, Ferrando R and Treglia G 2004 *Phase Trans.* **77** 101
[58] Kart H H, Yildirim H, Kart S O and Çağin T 2014 *Mater. Chem. Phys.* **147** 204
[59] Lee M S, Chacko S and Kanhere D G 2005 *J. Chem. Phys.* **123** 164310
[60] Stukowski A 2012 *Modelling Simul. Mater. Sci. Eng.* **20** 045021
[61] Ackland G J and Jones A P 2006 *Phys. Rev. B* **73** 054104
[62] Stukowski A 2010 *Modelling Simul. Mater. Sci. Eng.* **18** 015012